Institute of Physics Publishing Journal of Physics: Conference Series **53** (2006) 234–247
doi:10.1088/1742-6596/53/1/012 Corfu Summer Institute on Elementary Particle Physics

Prospects for B Physics at the Tevatron and LHCB

S. Donati
Istituto Nazionale di Fisica Nucleare, Largo Pontecorvo, 3, 56127 Pisa, Italy

Abstract. In this paper we will review the prospects for B physics analysis in the CDF experiment at the Tevatron collider and at the LHCB experiment.

1. INTRODUCTION

B hadrons are abundantly produced at the Tevatron Collider, the measured B^+ cross section is 3.6±0.6 μb in the region of transverse momentum $p_T(B^+) > 6.0$ GeV/c and rapidity $\mid \eta(B^+) \mid < 1$ [1]. This cross section is three orders of magnitude larger than at e^+e^- machines running at the $\Upsilon(4S)$ and the available energy allows the production of the heavier B_s^0, B_c and Λ_b hadrons. The challenge is extracting the interesting B signals from a level of background which is three orders of magnitude higher at production. This is achieved at CDF II with dedicated detectors and triggers.

2. THE TEVATRON COLLIDER

The Tevatron Collider collides 36 $p\overline{p}$ bunches at $\sqrt{s} = 1.96$ TeV. The design instantaneous luminosity was 10^{32} cm^{-2}s^{-1} but the Tevatron now exceeds it and set the peak luminosity record at 1.8×10^{32} cm^{-2}s^{-1}. With an already integrated luminosity of 1.3 fb^{-1}, the expectation is to have integrated ∼8 fb^{-1} by the year 2008.

3. THE CDF II DETECTOR

3.1. The tracking system

The CDF II tracker is located within a 14.1 kG solenoidal magnetic field and it is composed of silicon detectors and a drift chamber. There are three independent silicon detectors, SVXII, ISL and L00, for a total of eight silicon layers, 704 ladders and 722,432 channels [2]. SVXII is made of 360 double-sided ladders in a layout of six 15 cm axial sections × twelve 30° ϕ slices × five radial layers between 2.5 and 10.6 cm from the beamline. ISL covers the area between SVXII and the drift chamber, with 296 double-sided ladders at radii of 20 and 28 cm. With a length of 1.9 m, it provides silicon hits out to $\mid \eta \mid < 2$. L00 is a single-sided layer of 48 ladders mounted directly on the beampipe, 1.5 cm from the beamline, which enhances the track impact parameter resolution. The three subdetectors share the same readout system, starting with the SVX3D chip, a custom designed ASIC with a 128 channel × 42 capacitor analog storage ring, which makes it possible to acquire data in deadtimeless mode, integrating charge on one capacitor while reading out another one. The data acquisition system provides silicon data in time for Level 2 trigger processing. Over 90 % of the silicon detector is powered and more than 80 % is providing quality data. Charge collection efficiency is 99 % , with a single hit efficiency > 90 %.

The hit resolution for a two-strip cluster is 9 μm. The signal-to-noise ratio is above 10:1 both for $r-\phi$ strips and for $r-z$ strips.

The Central Outer Chamber (COT, [10]) is located outside the silicon detectors and inside the time-of-flight detector scintillators. The active volume of the COT spans 310 cm in the beam direction, 43.4 cm and 132.3 cm in radius, and the entire azimuth. The COT contains 30,240 sense wires that run the length of the chamber between two end plates. Approximately half of the wires are axial (run along the z direction) and half are small angle (2°) stereo. The $r-\phi$ view provides information for the p_T measurement, the $r-z$ view for the η measurement. The COT contains 96 sense wire layers in radius that are grouped into eight superlayers. Each superlayer is divided into supercells along the azimuthal angle, and each supercell has 12 sense wires and a maximum drift distance that is approximately the same for all superlayers. Therefore the number of supercells in a given superlayer scales approximately with the radius of the superlayer. The supercell layout consists of a wire plane containing sense and potential (or field shaping) wires and a field (or cathode) sheet on either side. Each field sheet is shared with the neighboring cell. The supercell is tilted by 35° with respect to the radial direction to compensate for the Lorentz angle of the drifting electrons in the magnetic field. The gas is a mixture or Ar/Et (50:50) and Isopropyl which provides a maximum drift time of 177 ns on the maximum drift distance of 0.88 cm. The measurement of the pulse widths provides a measurement of the dE/dx in the chamber, used for particle identification. The achieved performance of the integrated CDF II tracker is a transverse momentum resolution $\sigma(p_T)/p_T^2 = 0.15$ % (GeV/c)$^{-1}$ and an impact parameter resolution $\sigma(d) = 35$ μm @2 GeV/c. This performance is sufficient for the B physics analyses.

3.2. Particle identification detectors

CDF II uses two detectors and two complementary techniques for particle identification, one is the dE/dx measurement in the COT, the other one is the time-of-flight measurement in a dedicated detector. The COT readout electronics allows to measure the pulse width, which is related to the amount of charge collected by the wire. The truncated mean (80 %) computed on the hits associated to a track provides a measurement of the specific ionisation (dE/dx) in the chamber. A detailed calibration of the dE/dx measurement has been performed using samples of kaons and pions from $D^{*+} \to D^0\pi^+ \to [K^-\pi^+]\pi^+$, protons from $\Lambda^0 \to p\pi^-$, and muons and electrons from $J/\psi \to \mu^+\mu^-$ and $J/\psi \to e^+e^-$. The achieved K/π separation for $p_T > 2$ GeV/c is 1.4σ.

The Time-of-Flight detector (TOF, [4]) is istalled between the drift chamber and the solenoid magnet and extends 4.7 cm radially at a radius of roughly 138 cm. The detector is composed by Bicron scintillator bars BC-408, selected for the long (2.5 m) attenuation length. The bars have a dimension of 4×4 cm^2 in cross-section and 279 cm in length. There are a total of 216 bars, each covering 1.7° in ϕ and $|\eta|<1$. The photomultipliers are attached to each end of every bar. The time resolution on the single hit is 110 ps and the K/π separation is better than 2σ for $p_T < 1.5$ GeV/c. By combining the dE/dx and the time-of-flight measurements, the achieved K/π separation is better tha 1.4 σ in the entire momentum range.

3.3. Lepton detectors

Segmented electromagnetic and hadronic calorimeters surround the tracking system [6]. The electron energy is measured by lead-scintillator sampling calorimeters. In the central region ($|\eta|<1.1$) the calorimeters are arranged in a projective barrel geometry and measure electromagnetic energy with a resolution of $|\sigma(E_T)/E_T|^2 = (13.5\ \%)^2/E_T(GeV) + (2\ \%)^2$. In the forward region ($1.2<|\eta|<3.5$) the calorimeters are arranged in a projective end-plug geometry and measure the electromagnetic energy with a resolution of $|\sigma(E_T)/E_T|^2 = (14.4\ \%)^2/E_T(GeV) + (0.7\ \%)^2$. Both central and forward electromagnetic calorimeters are

instrumented with finely segmented detectors which measure the shower position at a depth where the energy deposition by a typical shower reaches its maximum. The central muon detector (CMU [5]) is located around the outside of the central hadron calorimeter at a radius of 347 cm from the beam axis. The calorimeter has a thickness of 5.5 interaction lengths and a ϕ segmentation of 15°. The muon drift cells are 226 cm long and cover 12.6° in ϕ, giving a ϕ coverage of 84 %. The pseudorapidity coverage is $\mid \eta \mid < 1$. Each module consists of four layers of four rectangular drift cells. The sense wires in alternating layers are offset by 2 mm for ambiguity resolution. The smallest unit in the CMU, called a stack, covers about 1.2° and includes four drift cells, one from each layer. Adjacent pairs of stacks are combined together to form a two-stack unit called a tower. A track segment detected in these chambers is called a CMU stub. A second set of muon chambers is located behind an additional 60 cm of steel. The chambers are arranged axially to form a box around the central detector. The coverage of the central muon system is extended to the region $0.6 < \mid \eta \mid < 1.0$ by four free-standing conical arches which hold drift chambers which cover 71 % of the solid angle.

4. THE CDF II TRIGGER

CDF II uses a three-level system to reduce the 1.7 MHz bunch crossing rate to 100 Hz written on tape. The Level 1 is a deadtimeless 7.6 MHz synchronous pipeline with 42 cells, which allows 5.5 μs to form a trigger decision. The maximum sustainable Level 1 output rate is 30 kHz. The Level 2 is an asynchronous pipeline with an average latency of 20 μs. While the events accepted by Level 1 are being processed by Level 2 processors, they are also stored on one of the four Level 2 buffers, waiting for Level 2 trigger decision. Each buffer is emptied when the Level 2 decision for the corresponding event has been asserted: if the event has been accepted, the buffer is read out, else it is simply cleared. If the Level 2 trigger decision takes too much time and the four buffers are all filled, the Level 1 accept is inhibited. This is a source of deadtime for the CDF II trigger. The maximum Level 2 output rate is 300 Hz. The Level 3 trigger is made of a CPU farm and has a maximum output rate of 100 Hz.

The heart of the Level 1 trigger is the eXtremely Fast Tracker (XFT, [7]), the trigger track processor that identifies high transverse momentum ($p_T > 1.5$ GeV/c) charged tracks in the transverse plane of the COT. The XFT tracks are also extrapolated to the calorimeter and to the muon chambers to generate electron and muon trigger candidates. Track identification in the XFT is accomplished in two processes by the Finder and by the Linker. The Finder searches for track segments in the four axial superlayers of the chamber. The Linker searches for a four-out-of-four or a three-out-of-four match among segments in the four layers, consistent with a prompt high-p_T track. The efficiency for finding XFT tracks is 96 %, with a transverse momentum resolution better than 2 % per GeV/c and azimuthal angular resolution of 5.5 mr. The level of fake tracks is 3 % at luminosity below 5×10^{31} cm^{-2}s^{-1} and grows with instantaneous luminosity.

The Online Silicon Vertex Tracker (SVT, [8]) is part of the Level 2 trigger. It receives the list of XFT tracks and the digitised pulse heights on the axial layers of the silicon vertex detector. The SVT links the XFT tracks to the silicon hits and reconstructs tracks with offline-like quality. In particular the resolution on the impact parameter, which is a crucial parameter to select B events since they tipically show secondary vertices, is 35 μm for 2 GeV/c tracks. The SVT efficiency is 85 % per track. Since a long Level 2 processing time can introduce dead time, to speed up operations the SVT has a widely parallelized design: it is made of 12 identical azimuthal slices working in parallel. Each slice receives and processes data only from one silicon vertex detector 30° sector. In addition SVT recontructs only tracks in the transverse plane to the beamline and only with $p_T > 2.0$ GeV/c. The tracking process is performed in two steps. The first step is the pattern recognition: candidate tracks are searched among a list of precalculated low resolution patterns. This is done in order to reduce the huge amount of silicon

hits only to those potentially interesting. The second step is track fitting: a full resolution fit of the hit coordinates found within each pattern is performed using a linearized algorithm. By providing a precision measurement of the impact parameter of the charged particle tracks, SVT allows triggering on events cointaining long lived particles, like the B events, which at the Tevatron have decay lengths of the order of 500 μm and produce tracks in the decay with impact parameters on average larger than 100 μm.

Level 3 trigger is implemented on a CPU farm which allows to perform an almost offline-quality event reconstruction.

4.1. Triggers for B physics

CDF II has basically three families of triggers for B physics: the dimuon trigger, the semileptonic trigger and the hadronic trigger.

The dimuon trigger selects muon pairs with transverse momenum as low as 1.5 GeV/c. It is mostly used to select J/ψs and $\psi(2S)$, to reconstruct the many decay modes of the B hadrons (B^0, B^+, B_s^0, B_c, and Λ_b) containing a J/ψ decaying to muon pairs, and to select $\Upsilon \to \mu^+\mu^-$ decays, or muon pairs for the search of the rare $B \to \mu^+\mu^- X$ decays, or for $b\overline{b}$ correlation studies.

The semileptonic trigger selects events with a lepton (μ or e) with $p_T > 4$ GeV/c and an SVT track with $p_T > 2$ GeV/c and impact parameter above 120 μm.

The hadronic trigger selects track pairs with $p_T > 2$ GeV/c and $p_{T1} + p_{T2} > 5.5$ GeV/c, with an opening angle in the transverse plane below 135°, impact parameter above 100 μm, a decay length above 200 μm. For the two-body decay trigger path, optimised to collect $B \to h^+h'^-$ decays, the track pair is requested to point back to the primary vertex, by requiring that the impact parameter of the reconstructed B is below 140 μm. To select hadronic multibody decays, like $B_s^0 \to D_s^-\pi^+$, the request on the pointing back to the primary vertex has low efficiency, since the track pair provides only a partial reconstruction of the multibody decay, and it is not applied.

The Tevatron performance has been continuosly improving since the beginning of Run II. At the time of writing these proceedings, the initial instantaneous luminosity of the stores may reach 1.8×10^{32} cm^{-2}s^{-1}, which is almost a factor of of two above design luminosity (10^{32} cm^{-2}s^{-1}), and the stores can last up to 30 hours, when they are dropped at an instantaneous luminosity around 2×10^{31} cm^{-2}s^{-1}. This is a factor of 9 decrease with respect to the initial store luminosity. If the trigger bandwidth is filled at the initial luminosity, it will get less and less occupied as the store luminosity decreases. So the problem is to adjust the trigger selections in order to have all the available bandwidth completely used at all instantaneous luminosities. This is achieved by implementing more versions of the same trigger with increasingly tighter cuts, and consequently increasing purity, and running the versions with tighter cuts with no prescale and the versions with looser cuts with a prescale. For the hadronic trigger the tighter version requires track pairs with $p_T > 2.5$ GeV/c and $p_{T1} + p_{T2} > 6.5$ GeV/c. The prescales can be made dynamical, and they adjust themselves as the luminosity decreases and more bandwidth becomes available. In addition to this, triggers are luminosity enabled: if the rate of a trigger that is important to keep unprescaled is too large at the initial luminosity, it is enabled only when the luminosity has decreased below a safe threshold.

4.2. Trigger upgrades

The CDF II trigger was designed for an instantaneous luminosity of 10^{32} cm^{-2} s^{-1}. The increase above this limit already achieved and the expectation to reach 3×10^{32} cm^{-2} s^{-1} demanded an upgrade of the system. The increased occupancy of the detectors, in particular of the COT, results in the increase of the rate of fake tracks in XFT, and consequently in the increase of the Level 1 triggers which use XFT tracks. The increased complexity of the events deriving from

the pile up of more interactions in the same bunch crossing, results in the increase of the SVT processing time and consequently in the increase of the trigger deadtime. The XFT is being upgraded to perform a three dimensional track recontruction and the SVT has been upgraded to use faster and more performant components.

5. The upgrade of the eXtremely Fast Tracker

The eXtremely Fast Tracker [9] finds tracks in the transverse plane of the CDF II Central Outer Chamber (COT) [10] in time for the Level 1 trigger decision. The XFT tracks are also matched to electromagnetic-calorimeter clusters for online electron identification, and to stubs in the muon system for muon identification. The role of the XFT in the trigger is to provide useful information to reduce the raw collision rate (1.7 MHz) to a maximum of about 30 KHz of more "interesting" physics events which can be processed by the Level 2 trigger. The XFT currently uses hit data from the 4 axial superlayers of the COT, which are arranged in cells of 12 wires each, for a total of 16,128 axial wires. A charged track passing through an axial layer generates a characteristic pattern of 12 hits, one per wire, with a characteristic timing. Track identification is performed in two processes by the Finder, which searches for track segments in each of the 4 axial layers of the chamber, and by the Linker, which searches for 4/4 as well as 3/4 matches among segments in the 4 layers, consistent with a track exiting from the interaction point. The XFT measures the transverse momentum and azimuthal angle of all the tracks with $p_T > 1.5$ GeV/c with an efficiency greater than 96 % per track, and resolution $\sigma_{p_T}/p_T^2 \sim 2\%$ (GeV^{-1}) and $\sigma_\phi \sim 6$ mR.

5.1. System architecture

The XTC mezzanine cards reside on the COT TDC's and classify the hits on each COT wire as prompt or delayed depending on whether the time of the hit is smaller or larger than 44 ns, respectively. These data are sent to a transition module on the back of the COT TDC crate and are sent at 45.5 MHz as LVDS signals to the Finder module crates, where they are received by transition modules and go to the Finder modules through a customized backplane. The Finder modules find track segments and transmit them to the Linker modules which find the tracks and the associated parameters p_T and ϕ. Track information is driven by transition modules to the extrapolation unit (XTRP) which extrapolates the tracks to the electromagnetic calorimeter and the muon chambers and distributes the data to the Level 1 and Level 2 triggers. At Level 2 the XFT tracks are used as seeds by the Online Silicon Vertex Tracker [14] which performs a combined track reconstruction in the tracking chamber and in the silicon vertex detector.

5.2. The upgrade of the system

The XFT was designed to perform online tracking at an instantaneous luminosity of about 10^{32} cm^{-2} s^{-1}. The increase above this limit demands an upgrade of the system to cope with the increased occupancy of the chamber, which results in a higher level of fake tracks and consequently in larger rates of the triggers based on the XFT tracks. The upgrade foresees that the existing axial system is not altered, and new Stereo Finder boards are added to find track segments in the three outer stereo layers of the COT. The idea is to reject fake axial tracks by requiring the association of the axial tracks with the stereo segments. The stereo upgrade also allows the measurement of the track parameters cot θ and z_0, which can be used to require the XFT track to point in the z-direction towards the calorimeter tower or the muon stub involved in electron or muon triggers.

5.3. Upgraded system architecture

The XTC-2 mezzanine cards reside on the TDC's that process data from the COT stereo layers. The card classifies the hits in 6 time windows with programmable edges, set around

55, 79, 103, 127, 151 and 255 ns. Data are transmitted through additional mezzanine cards installed at the back of the TDC crates to the Stereo Finders using optical fibers. The Stereo Finder boards identify track segments in the stereo layers of the COT. Each board covers a 30° azimuthal angle slice, so a total of 36 boards is necessary to instrument the 3 outer stereo layers. The number of 12 wire cells processed by each board is respectively 20/28/36 for the internal/central/external stereo layers. The Stereo Finder logic is implemented with two Altera Stratix EP2S60 Programmable Gate Arrays. The Stereo Finders output the list of found pixels, which indicate the position and slope of an identified track segment. The pixels exist in two formats output through two independent data streams on optical fibers. The first one has each COT cell divided in 12 pixels, with 6 azimuthal bins and 2 slope bins, and is directed to the Stereo Linker Association Modules (SLAM), which perform the matching between the axial XFT tracks and the stereo pixels. The second one, less compressed, has each COT cell divided in 90 pixels, with 18 azimuthal bins and 5 slope bins, and is directed to the Level 2 trigger processors, where the extra time available allows the use of more refined information. Each SLAM receives the axial track data from one Linker Module, which covers a 15° azimuthal angle slice, and the stereo pixels from a slice of 45° azimuthal angle covered by two Stereo Finders and centered on the region covered by the Linker Module. The association algorithm is implemented using one Altera Stratix EP1S25 per module. The format of the data output from the SLAM to the extrapolation unit (XTRP) is identical to the original output of the Linker Output Modules, with the insertion of the "matched/unmatched track" information and the "positive/negative z direction" in two presently spare bits. At high luminosity only matched tracks will be used in the trigger selection. The more precise stereo pixels transmitted to the Level 2 trigger are matched to the axial XFT tracks, and are used to measure the track cot θ and z_0, respectively with a resolution of ~ 0.1 and 10 cm, sufficient to improve the quality of the Level 2 selection.

6. Prospect for B physics at CDF

In the following sections we will review some of the most recent and most interesting results achieved by CDF, with some discussion on the prospects for these measurements with the statistics expected for run II.

7. Charmless B decays at CDF

The charmless decays of the b hadrons provide one of the most stringent tests of the CKM matrix and potential windows to New Physics effects. While several decays of the B^0 and B^+ mesons have already been measured at the $\Upsilon(4S)$, the Tevatron offers unique access to the B_s^0 and Λ_b^0 decays. The analyses reviewed here have been performed by using a $\approx$180 pb^{-1} data sample recorded by the CDF II experiment at the Tevatron $p\overline{p}$ collider, using the hadronic trigger based on SVT.

8. Measurement of branching fractions and CP asymmetries in $B^0 \to h^+h'^-$

This analysis uses the data collected by the trigger optimised for two-body decays. In the offline selection, to enhance the purity of the sample, further cuts are imposed on transverse momenta and impact parameters of the two tracks, and on transverse decay length, impact parameter and isolation of the B candidate. Isolation is defined as $\frac{p_T(B)}{p_T(B)+\sum p_T}$, where the sum runs on every other track within a cone of radius 1 in η-ϕ space around the B candidate flight direction. This cut is particularly effective in rejecting combinatoric background. The set of cuts is chosen to maximise the quantity $S/(S+B)^{1/2}$,where S is the number of expected signal events estimated from a detailed detector and trigger simulation using GEANT [19], and B is the background estimated by extrapolating the sidebands. The resulting invariant mass distribution computed

by assigning the pion mass to both tracks is reported in Figure 1, which shows a clean peak with 893±47 signal events, with width 38±2 MeV/c^2 and a peak S/B better than 2.

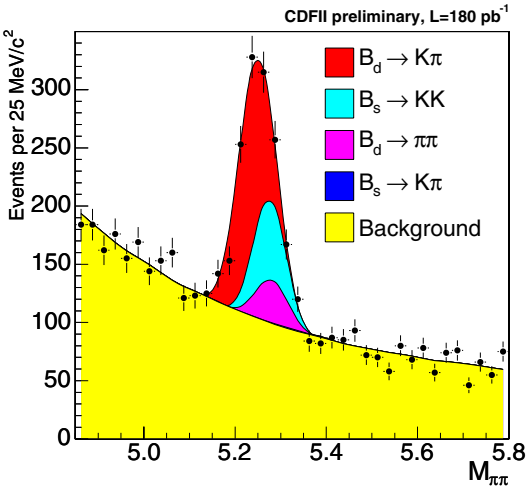

Figure 1. $B^0 \to h^+h'^-$ mass distribution computed with the pion mass assignment to both tracks. The contributions of the signals and of the background, as determined from the fit, are reported in different colors.

The simulation predicts sizeable signals in this mass region from B^0 and B_s^0 two-body decays: $B^0 \to K^+\pi^-$, $B^0 \to \pi^+\pi^-$ and $B_s^0 \to K^+K^-$, $B_s^0 \to K^-\pi^+$, overlapping into a single unresolved bump. The relative fractions of each $B_{d,s} \to h^+h'^-$ mode, along with the direct CP asymmetry in the self tagging mode $B^0 \to K^+\pi^-$, are determined with an unbinned likelihood fit which combines kinematic and particle identification information. The likelihood for event i is written as

$$L_i = (1-b)\sum_j f_j L_j^{kin} L_j^{PID} + bL_{bck}^{kin} L_{bck}^{PID} \tag{1}$$

where the index j runs on the signal modes and the parameters f_j are their relative fractions determined by the fit and b is the background fraction.

The kinematic term is $L_j^{kin} = P_j(M_{\pi\pi}|\alpha)P_j(\alpha, p_{tot}) = G(M_{\pi\pi} - M_j(\alpha), \sigma_M)P_j(\alpha, p_{tot})$. $M_j(\alpha)$ is obtained by solving for $M_{\pi\pi}$ the following approximate expression for the invariant mass of a particle pair:

$$M_{h_1h_2}^2 \approx M_{\pi\pi}^2 + (1+\frac{p_1}{p_2})(m_2^2 - m_\pi^2) + (1+\frac{p_1}{p_2})(m_1^2 - m_\pi^2) \tag{2}$$

The variable $\alpha = (1 - p_1/p_2)q_1$ is the signed momentun imbalance of the decay. p_1 (p_2) is the smaller (larger) track momentum and q_1 is the charge of the smaller momentum track, and $p_{tot} = p_1 + p_2$ is the scalar sum of the momenta of the two tracks. G is a gaussian distribution and $P_j(\alpha, p_{tot})$ is the joint probability distribution of α and p_{tot} for each signal mode after the effect of all reconstruction cuts. The $P_j(\alpha, p_{tot})$ are parameterised by product of polynomial and exponential functions using Monte Carlo samples.

The particle identification information is based on the dE/dx measurement in the drift chamber and it is summarised in the single observable $\mathtt{i} = (\frac{dE}{dx_{meas}} - \frac{dE}{dx_\pi})/(\frac{dE}{dx_K} - \frac{dE}{dx_\pi})$ for each track. dE/dx_K (dE/dx_π) is the expected dE/dx value of the track in the kaon (pion) mass hypothesis. The probability distribution of $\mathtt{i}$ is almost independent on momentum for kaons and pions. In the likelihood $L_j^{PID} = pdf_j^{PID}(\mathtt{i}_1, p_1(\alpha, p_{tot}), \mathtt{i}_2, p_2(\alpha, p_{tot}))$ the probability distribution functions pdf_j^{PID} are determined by making use of a huge calibration sample of

$D^0 \to K\pi$ decays, tagged by the presence of a $D^{*\pm}$, collected by the multybody trigger. The fit takes into account the residual correlation in the dE/dx response of tracks in the same event, due to residual time-dependent baseline fluctuations in the drift chamber response. In the momentun range of interest the measured K/π separation is close to 1.4σ. The background is described by $L_{bck} = L^{kin}_{bck} \cdot L^{PID}_{bck}$, with the kinematic term $L^{kin}_{bck} = P_{bck}(\alpha, p_{tot}) \cdot (e^{c_0+c_1 \cdot M_{\pi\pi}} + c_2)$, where $P_{bck}(\alpha, p_{tot})$ is parameterised from the sidebands of real data and the c_i are free parameters determined by the fit. The likelihood term related to particle identification for background is similar to the signal one and assumes that the background is composed of pions, kaons, protons and electrons, while muons are indistinguishable from pions with the available resolution.

The fit returns raw relative fractions which need to be corrected for the different efficiencies of the selection cuts for each decay mode in order to provide measurements of branching fractions. Part of the effects determining the different efficiencies are estimated using the detector simulation, part using real data, this has been done in particular for the efficiencies of the B isolation cut, for the relative efficiency of the trigger track processor for kaons and pions and for the detector charge asymmetry.

8.1. Results and prospects for run II

In the B^0 sector the measurements of the relative branching fraction $\frac{BR(B^0 \to \pi^+\pi^-)}{BR(B^0 \to K^+\pi^-)} = 0.21 \pm 0.05(stat.) \pm 0.03(syst.)$ and of the direct CP asymmetry $A_{CP}(B^0 \to K^+\pi^-) = -0.022 \pm 0.078(stat.) \pm 0.012(syst.)$ are compatible with the measurements performed by BaBar and Belle [15]. In the B^0_s sector the measurement of $\frac{f_s \cdot BR(B^0_s \to K^+K^-)}{f_s \cdot BR(B^0 \to K^+\pi^-)} = 0.46 \pm 0.08(stat.) \pm 0.07(syst.)$ allows to extract the absolute branching fraction $BR(B^0_s \to K^+K^-) = 31.1 \pm 5.4(stat.) \pm 5.2(syst.)$ by using the world average of the branching fraction of the $B^0 \to K^+\pi^-$. No evidence is found for the $B^0_s \to K^-\pi^+$ decay and the resulting limit is $BR(B^0_s \to K^-\pi^+) < 5.4 \cdot 10^{-6}$ @90% C.L..

Limits on rare modes dominated by penguin annihilation and exchange diagrams have been searched for by adding their expected contributions to the likelihood. No evidence is found for these modes. The limits are $BR(B^0 \to K^+K^-) < 1.82 \cdot 10^{-6}$ @90 % C.L. and $BR(B^0_s \to \pi^+\pi^-) < 1.6 \cdot 10^{-6}$ @90 % C.L and improve a previous CDF II result [16]. It will be interesting to be able to measure these unknown amplitudes, since they contribute to many relevant processes as the $B^0_s \to K^+K^-$ decay.

It is possible to extrapolate the resolution expected on the several measurements as more statistics becomes avalailable. In the 1 fb^{-1} dataset currently available we expect of the order of 6000-7000 $B^0 \to h^+h'^-$ events. For $A_{CP}(B^0 \to K^+\pi^-)$ we expect a resolution of the order of 2.5 % in 1 fb^{-1} of data and of the order of 1 % with all the expected run II data (8 fb^{-1}). For $\frac{f_s \cdot BR(B^0_s \to K^+K^-)}{f_s \cdot BR(B^0 \to K^+\pi^-)}$ we expect a statistical resolution of the order of 2 % in 1 fb^{-1} and a reduction of the systematic error from the improvement of the dE/dx calibrations. For the rare decay $B^0_s \to K^-\pi^+$, the theory expects a large direct CP asymmetry. Experimentally this decay mode shows the relevant feature of being self-tagging, which simplifies the measurement of direct A_{CP}. Both the measurement of branching fraction and A_{CP} may give a stringent test of validity of theoretical models and overconstrain the CKM parameters. Work is now in progress to perform these measurements in the 1 fb^{-1} dataset.

9. Search for $\Lambda^0_b \to h^+h'^-$ decays

Theoretical predictions for the $\Lambda^0_b \to pK$ and $\Lambda^0_b \to p\pi$ branching fractions lie in the range (1.4-1.9)$\times 10^{-6}$ for pK decays and (0.9-1.2)$\times 10^{-6}$ for $p\pi$ decays [17]. The $\Lambda^0_b \to ph^-$ branching ratio has been normalised to the branching ratio BR($B^0_d \to K\pi$)= $(1.85 \pm 0.11) \times 10^{-5}$ [18], which is a topologically similar decay. The relationship between the number of events (N) and branching fractions of the signal and normalising mode are given by: BR($\Lambda^0_b \to ph^-$) = $N(\Lambda^0_b \to ph^-)/A$

and $A = \frac{\epsilon_\Lambda}{\epsilon_B} \cdot \frac{f_\Lambda}{f_d} \cdot \frac{R \cdot N(B \to h^+ h'^-)}{BR(B_d^0 \to K\pi)}$ where ϵ_Λ (ϵ_B) is the total efficiency of observing a Λ_b^0 (B_d^0) and f_Λ (f_d) is the b-quark hadronization fraction of the Λ_b^0 (B_d^0). We use $f_\Lambda = 0.099 \pm 0.017$ and $f_d = 0.397 \pm 0.010$ [18], for a resulting value of $f_\Lambda / f_d = 0.25 \pm 0.04$. The efficiencies are estimated with the simulation of the detector and of the trigger. R is the relative fraction $N(B_d^0 \to K\pi)/N(B \to h^+ h'^-)$ measured in the $B^0 \to h^+ h'^-$ analisys.

The search has been performed with a blind analysis, by hiding the data in the signal mass region. The signal region is unblinded only after fixing all the selection criteria and estimating the systematic unsertainties. The background level is estimated by fitting the invariant mass spectrum and interpolating in the blinded signal region. Possible biases in the background estimate due to the cut optimisation procedure are avoided by splitting the full sample in two statistically independent subsamples and using one subsample for the cut optimisation and the other subsample for the measurement of the background level. Figure 1 shows the invariant mass distribution after all the selection criteria are applied, with the dotted line indicating the blinded region where a signal is expected. The solid line indicates the fit region used to determine the expected background level. In the search region also the Monte Carlo distributions of the $\Lambda_b^0 \to p\pi$ and $\Lambda_b^0 \to pK$ signals are reported. From the plot it is clear that the main source of background in the search window is combinatoric, while the contribution from the $B \to h^+ h'^-$ is negligible.

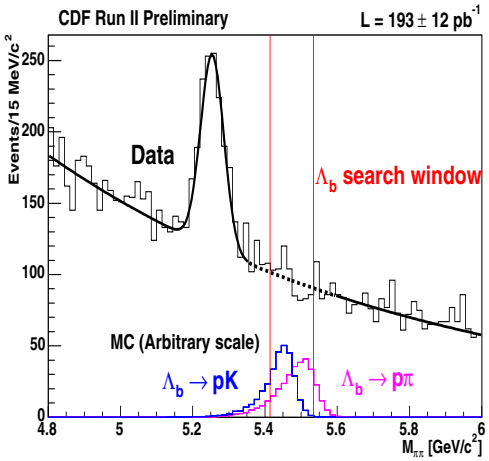

Figure 2. Di pion invariant mass distribution. The fitting function is used to extract the number of $B \to h^+ h'^-$ and background events. The dashed curve is the extrapolation of the fitting function in the region not used to perform the fit. The scales of the Monte Carlo signal distributions are arbitrary.

The selection cuts and the position of the search window have been determined from an optimisation procedure applied using the first subsample. The figure of merit $S/(1.5+\sqrt{B})$ [20], where S and B are respectively the signal and background events, is maximised. B is determined by extrapolating the fit performed in the sidebands (4.8 - 5.335 GeV/c^2 and 5.595 - 6.0 GeV/c^2) to the search window. In the formula the constant has been chosen in order to favor selections maximising the sensitivity reach at 3σ significance. When the background is large, as in our case, this expression reduces to the usual $S/\sqrt{B}$, while it reduces to $s/1.5$ when the background is low. In both cases it reduces to $\epsilon_\Lambda/(1.5+\sqrt{B})$, where ϵ_Λ is the signal efficiency determined with Monte Carlo. The optimised cuts require $\mid d_\Lambda \mid < 50$ μm, $L_{xy}(\Lambda) > 400$ μm and $min(\mid d_{01} \mid, \mid d_{02} \mid) > 180$ μm, and the optimised search window is determined to be between 5.415 and 5.535 GeV/c^2.

The expected background is determined using the second subsample and fitting the shape of the mass distribution with a combination of a gaussian for the $B \to h^+h^{'-}$ signal and some combinations of exponential and polynomial functions for the combinatoric background. The estimate is 772±31 expected background events in the Λ_b^0 search window and 726±82 $B \to h^+h^{'-}$ events, where the quoted error includes both the statistical error and the systematic error estimated as the fluctuation of the yields for different choices of the background model. The relative efficiency $\epsilon_\Lambda/\epsilon_B$ is estimated with Monte Carlo samples of $\Lambda_b^0 \to ph^-$ and $B_d^0 \to K\pi$. The total number of events in the signal region is 767, consistent within the error with the predicted background, 772±31. Upper limits on the branching fractions can be calculated using a Bayesan method with uniform prior distribution, taking into account both statistical and systematic uncertainties. The most relevant sources of systematic error are the uncertainty on the $B \to h^+h^{'-}$ yield, on the background estimate, on the relative efficiency $(\epsilon_\Lambda/\epsilon_B)$ correction factor and on f_Λ/f_d. The resulting upper limits are 2.3×10^{-5} at 90% C.L. for $\Lambda_b^0 \to pK^-$ and 2.9×10^{-5} at 90% C.L. for $\Lambda_b^0 \to p\pi^-$ [21]

10. Measurement of A_{CP} in the $B^+ \to \phi K^+$ decay and first evidence of the $B_s^0 \to \phi\phi$ decay

This analysis has been performed using the data collected by the multybody trigger. To cancel the uncertainty on the B production cross section and to reduce systematic uncertainties on detector efficiencies, the branching fractions are extracted from ratios of the decay rates of interest normalized to the well established and topologically similar $B_s^0 \to J/\psi\phi$ and $B^+ \to J/\psi K^+$ decay modes.

B candidates are reconstructed first by detecting $\phi \to K^+K^-$ and $J/\psi \to \mu^+\mu^-$ decays. Background from mismeasured tracks is reduced by requiring a good vertex χ^2, while combinatoric background is reduced by exploiting several variables sensitive to the long lifetime, relatively hard p_T spectrum of B mesons and the isolation of the B hadrons inside the b-quark jets. The cut values are optimized by maximizing the usual $S/\sqrt{S+B}$ for the already observed $B^+ \to \phi K^+$ signal and $S/(1.5+\sqrt{B})$ for $B_s^0 \to \phi\phi$ whose branching ratio is unknown. While the signal S is derived from Monte Carlo, the background B is estimated from the ϕ sideband $(1.04 < m_{KK} < 1.06$ GeV/c$^2)$ appropriately normalized.

The $B^\pm \to \phi K^\pm$ yield and A_{CP} are extracted simultaneously from an extended unbinned maximum likelihood fit on four variables to the combined B^+ and B^- sample: the three-kaon invariant mass, the invariant mass of the ϕ candidate, the cosine of the ϕ meson helicity angle and the measured dE/dx deviation from the expected value for pions for the lowest momentum trigger track. The likelihood function has seven components: signal, partially reconstructed $b \to \phi X$ decays, combinatoric background, $B^+ \to K^{*0}(892)\pi^+$, $B^+ \to f_0(980)\pi^+$, non-resonant $B^+ \to K^+K^-K^+$ and non-resonant $B^+ \to K^+\pi^-\pi^+$. For each component the likelihood function is the product of four one-dimensional probability distribution functions of the fit variables, assumed to be uncorrelated, which are parameterised from a combination of Monte Carlo simulation and sideband data. The measured value is $A_{CP} = -0.07 \pm 0.17^{+0.03}_{-0.02}$ [22]. The branching fraction is measured relatively to the $B^+ \to J/\psi K^+$ mode, which is reconstructed with the same requirements as the $B^+ \to \phi K^+$ candidates except for the invariant mass of the two muons being within 100 MeV/c^2 of the J/ψ mass. ¿From the $B^+ \to \phi K^+$ yield (47.0±8.4 events) and the $B^+ \to J/\psi K^+$ yield (439±22 events) and the correction for the relative trigger and reconstruction efficiciency between the two modes, it is measured $BR(B^+ \to \phi K^+) = (7.6 \pm 1.3(stat.) \pm 0.6(syst.)) \times 10^{-6}$ [22].

The $B_s^0 \to \phi\phi$ signal is selected requiring two pairs of kaons with an invariant mass within 15 MeV/c^2 of the world average ϕ mass. The search is performed in a blind way fixing the selection requirements and evaluating the combinatoric background from independent samples before examining the signal region in the data. In a region of ±72 MeV/c^2 around the world

average B_s^0 mass, corresponding to a window three times the expected mass resolution, 8 events are observed. The combinatoric background and the reflection from $B^0 \to \phi K^{*0}$, where the pion from the K^{*0} is assigned the kaon mass, are the two main sources of background expected in the B_s^0 signal region. After subtracting these two contributions, the signal yield is $7.3^{+3.2}_{-2.5}$ events, and the resulting one-sided Gaussian significance of the signal is 4.7σ. The $BR(B_s^0 \to \phi\phi)$ is measured relative to the $B_s^0 \to J/\psi\phi$ decay, reconstructed requiring one pair of kaons and one pair of muons within 15 and 50 MeV/c^2 of the world average ϕ and J/ψ mass respectively, and applying the other kinematic selection criteria similar to the $B_s^0 \to \phi\phi$ mode. As in the $B^+ \to \phi K^+$ case, the $B_s^0 \to \phi\phi$ decay rate is derived from the $B_s^0 \to \phi\phi$ yield, from the $B_s^0 \to J/\psi\phi$ yield and the relative efficiency between the two modes. It is measured $BR(B_s^0 \to \phi\phi) = (14^{+6}_{-5}(stat.) \pm 6(syst.)) \times 10^{-6}$ [22], where the systematic error is dominated by a 36 % contribution due to the uncertainty on $BR(B_s^0 \to J/\psi\phi)$.

11. B_s^0 mixing measurements

CDF has recently presented the first measurement of the $B_s^0 - \overline{B}_s^0$ oscillation frequency Δm_s, using 1 fb^{-1} of hadronic data. The sample contains signals of 3,600 fully reconstructed hadronic B_s^0 decays and 37,000 partially reconstructed semileptonic B_s^0 decays. The probability as a function of proper decay time that the B_s^0 decays with the same, or opposite, flavor as the flavor production has been measured and a signal consistent with $B_s^0 - \overline{B}_s^0$ has been found. Under the hypothesis that the signal is due to $B_s^0 - \overline{B}_s^0$ oscillations, the value $\Delta m_s = 17.31^{+0.33}_{-0l.18}(stat.) \pm 0.07(syst)$ ps^{-1} has been measured and the value $\mid V_{td}/V_{ts} \mid = 0.208^{+0.001}_{-0.002}(exp.)^{+0.008}_{-0.006}(theo.)$ has been determined.

To reconstruct $\overline{B}_s^0$ candidates, we first select D_s^+ candidates. We use $D_s^+ \to \phi\pi^+$, $K^*(892)^0K^+$ and $\pi^+\pi^-\pi^+$, with $\phi \to K^+K^-$ and $K^{*0} \to K^+\pi^-$: we require that ϕ and K^{*0} candidates be consistent with the known masses and widths of these two resonances. These D_s^+ candidates are combined with one or three additional charged particles to form $D_s^+l^-$, $D_s^+\pi^-$ or $D_s^+\pi^-\pi^+\pi^-$ candidates. The D_s^+ and other decay productus of a $\overline{B}_s^0$ candidate are constrained to originate from a common vertex in three dimensions. For the $K^*(892)^0K^+$ final state, we remove candidates that are consistent with the decay $D^+ \to K^-\pi^+\pi^+$. We find signals of 3,600 hadronic B_s^0 decays and 37,000 semileptonic B_s^0 decays. The decay time in the B_s^0 rest frame is $t = K[L_T m_B/p_T]$, where L_T is the displacement of the B_s^0 decay vertex with repect to the primary vertex projected onto the B_s^0 transverse momentum vector. The facto K corrects for the missing momentum in the semileptonic decays ($K = 1$ for hadronic decays). The flavor of the B_s^0 at production is determined using both opposite-side and same-side flavor tagging techniques. The effectiveness $Q = \epsilon D^2$ of these techniques is quantified with an efficiency ϵ, the fraction of signal candidates with a flavor tag, and a dilution $D = 1 - 2w$, where w is the probability that the tag is incorrect. Opposite-side tags infer the production flavor of the B_s^0 from the decay products of the b hadron produced from the other b quark in the event. We use lepton (e and μ) charge and jet charge as tags, building on techniques developed for CDF run I measurements. The combined opposite-side tag effectiveness is $Q = 1.5 \pm 0.1$ %, where the undertainty is dominated by the statistics of the control samples. Same-side flavor tags are based on the charges of associated particles produced in the fragmentation of the b quark that produces the reconstructed B_s. In hte simplest picture of fragmentation, a π^+ (π^-) accompanies the formation of a B^- (B^+), a π^- (π^+) accompanies a $\overline{B}^0$ (B^0), and a K^- (K^+) accompanies a $\overline{B}_s^0$ (B_s^0). In this analysis we use dE/dx and time-of-flight information in a combined particle identification likelihood to indentify the kaons associated with the B_s production. Tracks close in phase space to the B_s candidate are considered as same-side kaon tag candidates, and the track with the largest kaon likelihood is selected as the tagging track. The effectiveness of this flavor tag is $Q = 3.5$ % (4.0 %) in the hadronic (semileptonic) decay sample. The fractional

undertainty on Q is approximately 25 %.

We use an unbinned maximum likelihood fit to search for B_s oscillations. The likelihood combines mass, decay time, decay-time resolution and flavor tagging information for each candidate, and includes terms for signal and each type of background. The fit finds $\Delta m_s = 17.31^{+0.33}_{-0.18}(stat.) \pm 0l.07(syst.)$ ps^{-1}. It is possible to derive $\mid V_{td}/V_{ts} \mid = 0.208^{+0.001}_{-0.002}(exp.)^{+0.008}_{-0.006}(theo.)$. The precision of the Δm_s measurement is now better than 2 % and the value of Δm_s is consistent with Standard Model expectations and with previous bounds, and it allows to improve constraints on the unitarity of the CKM matrix and on the scenarios involving new physics. As the available statistics increases, it will be possible to improve the quality of this measurement.

12. Properties of the B_c meson

The B_c meson is the ground state of b and c quarks which makes it a unique system with two heavy quarks of different flavors. The presence of both such quarks impacts on the production, decay and mass properties of the B_c meson. The B_c meson is expected to have decay properties that include both a shorter c-like lifetime and a large number of possible final states. The measurement of the mass of the B_c is interesting to compare with theoretical predictions using potential models, and lattice QCD calculations. CDF has analysed data in semileptonic decays, $B_c^- \rightarrow J/\psi l^- X$, both electron and muon channels, and also in the hadronic decay $B_c^- \rightarrow J/\psi\pi^-$, where $J/\psi \rightarrow \mu^+\mu^-$. In the semileptonic decay channel, a total of 106 candidates are observed from the analysis of 360 pb^{-1}. The several sources of backgorund are estimated and the signal shows an excess of 5.2σ. The produciton cross section times branching ratio with respect to the $B^+ \rightarrow J/psiK^+$ has been measured as $R = 0.249\pm0.045\pm0.069^{0.082}_{-0.033}$ with $p_T(B) > 4$ GeV/c and $\mid y \mid < 1$. CDF has studied also the $B_c \rightarrow J/\psi e\nu X$ and performed a lifetime measurement in this decay mode. From an unbinned likelihood fit, the lifetime of the B_c meson has been measured as $\tau(B_c) = 0.463^{+0.073}_{-0.065} \pm 0.036$ ps. CDF reported evidence of $B_c^- \rightarrow J/\psi\pi^-$ decay from 360 pb^{-1}, with a recent mass measurement performed in this channel using 1.1 fb^{-1} of data. The mass measurement is doable since the decay channel is fully reconstructed. The analysis estimates 49.1±9.7 B_c signal events over a background of 34.1 events, which corresponds to a significance larger than 6.5σ. An unbinned maximum likelihood fit is used to extract the mass of the B_c meson as $M(B_c) = 6276.5 \pm 4.0 \pm 2.7$ MeV/c^2, compared to the prediciton from lattice QCD calculation of $M(B_c)_{LAT} = 6304 \pm 12^{+18}_{-0}$ MeV/c^2. The study of the B_c phenomenology will significantly benefit from the use of all the statistics available in run II.

13. Search for $B^0_{(s)} \rightarrow \mu^+\mu^-$

In the Standard Model Flavor Changing neutral Current decays are highly suppressed and can only occur through higher order diagrams. The decay rate of the decay $B_s^0 \rightarrow \mu^=\mu^-$ is proportional to the CKM matrix element $\mid V_{ts} \mid^2$. The rate of $B_d \rightarrow \mu^+\mu^-$ is further suppressed by the ratio $\mid V_{td}/V_{ts} \mid^2$. The Standard Model expectations for these branching fractions are BR$(B_d \rightarrow \mu^+\mu^-) = (1.00\pm0.14)\times10^{-10}$ and BR$(B_s^0 \rightarrow \mu^+\mu^-) = (3.42\pm0.54)\times10^{-9}$, which are about two orders of magnitude smaller than the current experiemntal sensitivity. However, new physics contributions can significantly enhance these branching fractions. An observation of these decays at the Tevatron would be unambiguos evidence for physics beyond the Standard Model. The data used in this analysis are selected by the dimuon triggers. The offline reconstruction requires a confirmation of the two trigger muons of opposite charge whcih are constrained to exit from the same three-dimensional space point and are required to satisfy vertex fit quality criteria. ¿From the analysis of 780 pb^{-1} of dimuon data, CDF sets the following limits BR$(B_d \rightarrow \mu^+\mu^-) < 3.0 \times 10^{-8}$ @95% CL and BR$(B_s \rightarrow \mu^+\mu^-) < 1.0 \times 10^{-7}$ @95% CL. These limits will benefit from the continuous increase of statistics.

14. Status and B physics prospects at LHCb

The LHCb experiment will study CP violation and rare phenomena in the B hadron decays with very high precision. The experiment will be based at CERN and will study the decay of b quarks from $b\overline{b}$ pairs produced in proton-proton collisions. It will operate at a lower luminosity (2×10^{32}) than the the LHC design luminosity, in order to have on average one single interaction per crossing. This will simplify trigger design and event reconstruction and will reduce radiation damage on the detectors. Key elements of the detector are high track reconstruction efficiency, particle identification, vertexing and proper time resolution and high trigger efficiency.

14.1. The LHCb detector

The LHCb is a single-arm spectrometer with an angular coverage from 10 mrad to 300 (250) mrd in the bendind (non-bending) plane. The geometry is motivated by the kinematics of $b\overline{b}$ production in high energy proton-proton collisions. The key elements of the LHCb detector are:

- Acceptance down to small polar angles/large pseudo-rapidity, to maximise B-hadron yield;
- Excellent proper time resolution to exploit the full B physics potential at the LHC, including measurements in the rapidly oscillating B_s^0 system;
- Particle identification by two Ring Imaging CHerenkov (RICH) counters, for clean data samples and flavor tagging with kaons;
- Dedicated B trigger, including high p_T hadron and lifetime triggers for high efficiency.

The LHCb detector includes a vertex detector system, which includes the pile-up veto counter, a magnet and a tracking system; two RICH counters; an electromagnetic calorimeter and a hadron calorimeter, and a muon detector.

14.2. B physics prospects at LHCb

With its huge number of $b\overline{b}$ pairs, LHCb will be able to significantly improve the measurements (angle β, mass and lifetime of the CP eigenstates of the B_s^0 system, Δm_s and $\Delta\Gamma_s$) from the Beauty Factories and the Tevatron citerademacker. The LHCb plan is to perform precision measurements of the angle γ in many different decay channels both in the B_d and B_s^0 systems.

The decay $B_d \to \pi^+\pi^-$ is sensitive to the CKM angle γ, due to the $b \to u$ transition in the tree diagram. The presence of penguin contributions complicates the interpretation of the observed CP asymmetries in terms of CKM angles, but it is more interesting, since penguin diagrams are sensitive to the presence of new physics. A possible strategy that allows to disentangle the tree and penguin contributions and to measure γ is due to Fleischer [24] and usus E-spin symmetry of the strong interactions to relate the time-dependent CP asymmetries in the $B_d \to \pi^+\pi^-$ and $B_s^0 \to K^+K^-$ decays. LHCb can exploit its strong capabilities of kaon/pion separation to achieve the required sample purity. The expected precision on the measurement of the angle γ is 5°.

The $B_s \to D_s K$ and $B_d \to D^{(*)}\pi$ decay amplitudes do not have a penguin contribution [25]. These decays should measure the angle γ in a clean way. To reconstruct cleanly these decays the particle identification capabilities are crucial, in order to reduce the background from $B_s \to D_s\pi$, which has a ~ 10 times higher branching ratio. LHCb expects to reconstruct 5.4 k $B_s \to DK$ events per year with a background-to-signal of better than 0.5. The resulting sensitivity on γ is $\sim 15^\circ$.

The angle γ can be measured untagged, time-integrated samples of $B_d^0 \to \overline{D}^0 K^{*0}$. This method is sensitive to new physics in the D^0 oscillations. The expected precision on the measurement of γ is 8.2° with one year of data taking.

15. Bibliography

[1] D. Acosta et al., the CDF Collaboration, Phys. Rev. D **65**, 052005 (2002).
[2] A. Sill et al., Nucl. Instrum. Meth. A530:1 (2004).
[3] T. Affolder et al., Nucl. Instrum. Meth. A526:249 (2004).
[4] D. Acosta et al., Nucl. Instrum. Meth. A518:605 (2004).
[5] G. Ascoli et al., Nucl. Instrum. Meth. A268:33 (1988).
[6] L. Balka et al., Nucl. Instrum. Meth. A267:272 (1988). M. Alborw. et al., Nucl. Instrum. Meth. A453:84 (2000).
[7] E. J. Thomson et al., IEEE Trans. on Nucl. Sc. vol. 49, n. 3 (2002).
[8] A. Bardi et al., Nucl. Instrum. Meth. A485:178 (2002).
[9] E. J. Thomson *et al.*, IEEE Trans. Nucl. Sci. 49, 1063 (2002)
[10] T. Affolder *et al.*, Nucl. Instrum. Meth. A526: 249, (2004)
[11] W. Ashmanskas *et al.*, Nucl. Instrum. Meth. A518: 532, (2004)
[12] D. Acosta et al., Phys. Rev. D71, 032001 (2005).
[13] E. J. Thomson et al., IEEE Trans. Nucl. Sci. 49, 1063 (2002).
[14] W. Ashmanskas et al., Nucl. Instrum. Meth. A518, 532 (2004).
[15] J. Boyd, These Proceedings, G. Wei-ShuHou, These Proceedings.
[16] G. Punzi, for the CDF II Collaboration, FERMILAB-CONF-04-515-E.
[17] R. Mohanta, A. K. Giri and M. P. Khanna, Phys. Rev. D63, 074001 (2001).
[18] S. Eidelman et al.[Particle Data Group], Phys. Lett. B592, 1 (2004).
[19] R. Brun, R. Hagelberg, M. Hansroul, and J. C. Lasalle, reports no. CERN-DD-78-2-REV and CERN-DD-78-2.
[20] G. Punzi, in *Proceedings of PhyStat2003* (SLAC, 2003), arXiv:physics/0308063.
[21] D. Acosta et al., the CDF II Collaboration, arXiv:hep-ex/0507067.
[22] D. Acosta et al., the CDF II COllaboration, arXiv:hep-ex/0502044.
[23] J. Rademacker, hep-ex/0503001.
[24] R. Fleischer, Phys. Lett B **459** (1999).
[25] R. Aleksan, I. Dunietz and B. Kayser, Z. Phys. C **54** (1992).